Published in final edited form as:
Ind Eng Chem Res. 2013 August 7; 52(31): 10430–10440. doi:10.1021/ie400507c.

Reactive Functionalized Membranes for Polychlorinated Biphenyl Degradation

Minghui Gui[†], **Lindell E. Ormsbee**[‡], and **Dibakar Bhattacharyya**[†,*]

[†]Department of Chemical and Materials Engineering, University of Kentucky, Lexington, KY 40506

[‡]Department of Civil Engineering, University of Kentucky, Lexington, KY 40506

Abstract

Membranes have been widely used in water remediation (e.g. desalination and heavy metal removal) because of the ability to control membrane pore size and surface charge. The incorporation of nanomaterials into the membranes provides added benefits through increased reactivity with different functionality. In this study, we report the dechlorination of 2-chlorobiphenyl in the aqueous phase by a reactive membrane system. Fe/Pd bimetallic nanoparticles (NPs) were synthesized (in-situ) within polyacrylic acid (PAA) functionalized polyvinylidene fluoride (PVDF) membranes for degradation of polychlorinated biphenyls (PCBs). Biphenyl formed in the reduction was further oxidized into hydroxylated biphenyls and benzoic acid by an iron-catalyzed hydroxyl radical (OH•) reaction. The formation of magnetite on Fe surface was observed. This combined pathway (reductive/oxidative) could reduce the toxicity of PCBs effectively while eliminating the formation of chlorinated degradation byproducts. The successful manufacturing of full-scale functionalized membranes demonstrates the possibility of applying reactive membranes in practical water treatment.

Keywords

iron oxide; PVDF membrane; hydroxyl radical; catalysis; nanoparticles; Fenton reaction

1. Introduction

Membranes have been used as selective barriers for fluid separation based on size exclusion (sieving), charge (Donnan exclusion) and diffusion (solution-diffusion). In recent years, membrane functionalization (such as surface modification with functional groups) provides us an opportunity to incorporate catalytic nanoparticles (NPs) or enzymes in the membrane pores for in-situ reaction.[1–4] Iron-related NPs such as iron and iron oxide have drawn more and more attention in the detoxification of chlorinated organic compounds (COCs). These

[*]Corresponding Author: D. Bhattacharyya, University Alumni Professor, Department of Chemical & Materials Engineering, University of Kentucky, Lexington, KY 40506, db@engr.uky.edu, Phone No.: 859-257-2794.

Supporting Information Available

These include the pure water flux of Fe/Pd NP immobilized PVDF-PAA membrane; 2- chlorobiphenyl dechlorination by Fe/Pd NPs in aqueous phase; and GC-MS chromatographs and spectra of tentatively identified 3-; 4-hydroxybiphenyl, trihydroxybiphenyls and identified 2,2'-dihydroxybiphenyl and benzoic acid. This information is available free of charge via the Internet at http://pubs.acs.org.

compounds can be degraded into less toxic or nontoxic products by reductive[5–10] or oxidative pathway,[11–16] depending on the valence state of iron.

Zero-valent iron NPs have been extensively studied to reduce COCs in water by electron transfer reaction.[17] However, a second metal such as Pd or Ni is necessary to form bimetallic NPs (Fe/Pd or Fe/Ni) with iron to accomplish the complete removal of chlorine atoms from polychlorinated biphenyls (PCBs). The redox reaction between iron and water generates hydrogen (H_2), which is activated by Pd catalyst for hydrodechlorination.[9] On the other hand, iron oxide NPs are effective free radical catalysts in a heterogeneous Fenton reaction. The addition of hydrogen peroxide (H_2O_2) is required to produce the hydroxyl radicals (OH•).

Both reductive and oxidative pathways present challenges in the dechlorination of PCBs. The reductive method can only remove the chlorine atoms from the aromatic ring resulting in a biphenyl product, which is mildly toxic. The oxidative method is able to convert PCBs into the hydroxylated PCBs[18] followed by the aromatic ring cleavage,[19] eventually forming carboxylic acids or even carbon dioxide.[20] However, the chlorinated degradation byproducts formed by hydroxylation and the ring-opening reaction are still toxic and have higher water solubility than PCBs. Therefore, a combined pathway (Figure 1) is more beneficial in terms of first converting PCBs into biphenyl (reduction) by Fe/Pd NPs, followed by an oxidative treatment involving free radical generation. The toxicity of biphenyl is expected to be reduced without forming any chlorinated byproduct. We reported the synthesis of Fe,[21] Fe/Pd,[22–23] Fe/Ni[24] and iron oxide[25] immobilized polyvinylidene fluoride (PVDF)/ polyacrylic acid (PAA) membranes for trichloroethylene (TCE) and PCB dechlorination. These functionalized membranes have been used as the porous supporting materials to control NP synthesis (size, loading), to recapture the dissolved metal ions (ion exchange), to minimize the particle agglomeration (in-situ synthesis) and to allow the convective flow studies through pores (conversion control by residence time).[23, 26–27] Besides, they can be made into modules for real life application, and it's relatively easy to replace and regenerate the modules.

However, the possibility of using a combined pathway with iron immobilized membranes for PCB degradation has not been studied. The performance of membranes on the reduction of PCBs in aqueous phase and the byproducts formed during the oxidation of biphenyl are also unknown. Although our group has done extensive dechlorination studies on PCB congeners, 2-chlorobiphenyl has never been used as a model compound and it's an important intermediate in the dechlorination of 2,2'-dichlorobiphenyl.[23] The specific aims of this study include: (i) to study the responsive behavior of functionalized membranes; (ii) to evaluate the reactivity of Fe/Pd NPs in aqueous phase dechlorination of 2-chlorobiphenyl (batch and convective flow); (iii) to determine the reaction intermediates during the free radical oxidation of biphenyl; and (iv) to understand the subsequent oxidation mechanism.

2. Materials and methods

2.1 Materials

All chemicals used in the study were reagent grade without further purification. Sodium borohydride (99.99 %), titanium oxysulfate (99.99 %), and acrylic acid (99 %) were purchased from Sigma-Aldrich. Hydrogen peroxide (30 wt%), sodium hydroxide (1 M), sulfuric acid (0.5 M) and ferrous chloride tetrahydrate ($FeCl_2$•$4H_2O$) were obtained from Fisher Scientific. Ethanol (99.5 %), ammonium persulfate (98 %) and N,N'-methylenebisacrylamide (NNMA, 99 %) were purchased from Acros Organics. Hydrophilized PVDF microfiltration membranes (average pore size: 0.65 μm, thickness: 125 μm, porosity: 70 %, diameter: 142 mm) were obtained from Millipore. All of the solutions were prepared by deionized ultrafiltered water (DIUF) from Fisher Scientific. Deoxygenated water was obtained by purging N_2 into DIUF water for 30 min.

2.2 Methods

2.2.1 Membrane functionalization—PVDF membrane pores were functionalized by PAA which was formed via in situ polymerization of acrylic acid (AA) (Figure 2). The polymerization solution was composed of monomer acrylic acid (10 mL), initiator ammonium persulfate (0.33 g, 1 mol% of AA), cross-linker NNMA (0.22 g, 1 mol% of AA), and deoxygenated water (40 mL). PVDF membranes were dipped into the solution for 5 min, sandwiched between two glass plates after removing the solution on the external surface and put into the oven at 70 °C for 1 h. Thermal treatment accelerates both the polymerization and cross-linking reaction. N_2 was purged into the oven to remove O_2 which is an inhibitor of polymerization. Cross-linked PAA chains were formed inside the membrane pores. After the pore functionalization, the membranes were soaked in ethanol to dissolve the unreacted monomers and byproducts.

To establish that the functionalization steps could be scaled up, full-scale PVDF-PAA flat sheets and modules (40 inches wide and 300 feet long) were developed at Sepro Membranes Inc. in Oceanside, CA. The PVDF membrane (hydrophilized, average pore size: 0.42 μm, PVDF layer thickness: 70 μm compared to 125 μm for Millipore membrane; porosity: 45–55 %) was made with backing fabric polyester (highly open structure, thickness: 120 μm) to increase the material stability for ease of making spiral modules. The polymerization solution was similar as that used in the bench-scale study except the cross-linker (i.e. ethylene glycol) as well as a lower amount of acrylic acid to reduce the viscosity of solution. A small amount of PAA solution was also added to accelerate the formation of cross-linked polymer.

2.2.2 Fe/Pd bimetallic NP in-situ synthesis in functionalized membranes—Fe/Pd NPs were synthesized via ion exchange, borohydride reduction and palladium post coating procedure reported in our previous studies.[22, 28] PVDF-PAA membranes were soaked in NaCl (68.4 mM) solution for cation exchange. The ionized carboxyl groups chelated with Na^+ while releasing H^+. Therefore, NaOH was added to maintain the pH. After 12 h, the membranes were washed by deoxygenated water to remove the excess NaCl/NaOH inside the pores. They were then immersed in $FeCl_2$ solution (3.57 mM, pH=5.0–5.3)

for a second ion exchange with N_2 protection (4 h). Na^+ was replaced by Fe^{2+}, forming the iron-carboxylate bonds. Fe^{2+} was immediately reduced to zero-valent iron NPs when soaking the membranes in $NaBH_4$ solution (26.4 mM). The post coating of Pd NPs on iron surface was achieved by soaking the PVDF-PAA-Fe membranes in K_2PdCl_4 solution (153 μM, ethanol:water=9:1 v/v) for 2 h. Pd^{2+} were reduced by Fe^0, forming Pd^0 and Fe^{2+}. The membranes were washed with the deoxygenated water before use.

2.2.3 PCB dechlorination using Fe/Pd NPs (reductive pathway)—To determine the reactivity of NPs in membranes, 2-chlorobiphenyl was selected as a model compound and both batch and convective flow experiments were conducted. PCB stock solution was made by dissolving 2-chlorobiphenyl powders in deoxygenated water with heating (60 °C) and vigorous stirring using a TEFLON coated stir bar for one day. The solution was filtered through a regenerated cellulose ultrafiltration membrane (NMWL=100,000) before use.

A batch experiment was conducted in 20 mL EPA glass vials with shaking (300 rpm). The reaction started as the PVDF-PAA membranes (cut into small pieces with the external area of 17.3 cm^2) containing Fe/Pd NPs were soaked in PCB stock solution (20 mL). It was stopped by extracting solution and membranes separately with equi-volume hexane twice (2 h shaking).

A convective flow experiment was conducted in a solvent-resistant filtration cell (Sepa ST from GE Osmonics) with a nitrogen tank to supply the pressure. The feed solution was permeated through the Fe/Pd immobilized PVDF-PAA membranes (effective external area: 13.2 cm^2) and reacted with NPs inside the pores. The residence time of pollutants can be varied by changing the pressure in the cell. The permeate was collected and also extracted with hexane twice for gas chromatography-mass spectroscopy (GC-MS) analysis.

2.2.4 Biphenyl oxidation by heterogeneous Fenton reaction (oxidative pathway)—As the final product of PCB dechlorination, biphenyl is mildly toxic and requires further treatment to form less toxic products. Fe/Pd NPs were partially oxidized after reductive dechlorination due to the iron corrosion. However, both iron and iron oxide NPs are effective catalysts for heterogeneous Fenton reaction, in which OH• are generated from H_2O_2 decomposition for pollutant oxidation.[14, 29] Iron NPs can enhance the free radical generation by releasing Fe^{2+} during the oxidation of H_2O_2, while H_2O_2 was utilized more efficiently with iron oxide NPs.

2.3 Materials characterization

2.3.1 Membrane and particle characterization—A scanning electron microscopy (SEM, Hitachi S4300) coupled with an energy dispersive X-ray spectrometer (EDX) was used to observe the membrane pore size and analyze the particle composition on the surface and inside the pores of membranes. The membrane cross-section samples were obtained via freezing and fracturing the membrane in liquid nitrogen. X-Ray diffraction (XRD) analysis was performed with Cu-Ka (1.5418 Å) radiation using a Bruker-AXS D8 Discovery diffractometer to detect the material crystallography. A transmission electron microscopy (TEM, JEOL 2010F) coupled with an electron energy loss spectroscopy (EELS) were

utilized to study the oxidation of Fe NPs during H_2O_2 treatment. Line scan and elemental mapping were conducted using a scanning transmission electron microscopy (STEM) mode.

2.3.2 PCB and related compound analysis—2-Chlorobiphenyl and biphenyl were analyzed by GC-MS (Varian CP3800 GC with DB- 5 column and Saturn 2200 MS) with naphthalene-d8 as the internal standard. The calibration curve was made up of 12 points from 0.05 mg/L to 10 mg/L with R^2=0.999. The samples obtained in biphenyl oxidation were first acidified (pH 2) by sulfuric acid to make sure all organic acids formed were in their unionized form, followed by equi-volume extraction with hexane twice (2 h). All liquids in hexane phase were combined and concentrated under gentle N_2 flow, followed by the derivatization with N,O-Bis(trimethylsilyl) trifluoroacetamide (BSTFA) and pyridine (1:1 v/v, 200 μL). The average analytical error was less than 7 %. The efficiency of hexane extraction was 95±3 % for PCBs (including biphenyl) and 90±2 % for hydroxylated biphenyls (2- and 2,2'- dihydroxylbiphenyl).

2.3.3 Metal content analysis—The amount of Fe and Pd immobilized in the membranes during the ion exchange and post coating was quantified via material balance using a Varian spectra 220 fast sequential atomic absorption spectrometer (AAS). The Fe lamp was operated at the wavelength of 386.0 nm and the Pd lamp was at 247.6 nm. The results were checked by digesting the membranes in nitric acid (35 %) after reaction and analyzing the metal concentrations directly. The metal loss due to dissolution was also measured by AAS. The analytical error was less than 2 %.

2.3.4 H_2O_2 analysis—The concentrations of H_2O_2 were monitored based on a colorimetric method developed by Clapp et al.[30]. The samples were analyzed by Varian Cary Bio300 UV-Visible absorption spectroscopy with the detection at 407 nm. Titanium oxysulfate was added as the indicator (10 μL in 1 mL sample). The analytical error was less than 3 %.

3. Results and Discussion

The pH responsive behavior of functionalized membranes and its reversibility was proved by the flux modulation at different pH values. 2-Chlorobiphenyl was successfully degraded via the combined pathway treatment. The intermediates detected were hydroxylated biphenyls and benzoic acid.

3.1 PVDF-PAA Membrane and Fe/Pd NP properties

The in-situ polymerization of acrylic acid inside PVDF membrane pores was conducted in the aqueous phase with no organic solvent involved. The cross-linking reaction between PAA chains via NNMA bonding created a very stable polymer network, which would not collapse under acidic or alkaline environment. PVDF is well-known for its excellent chemical resistance to most acids, weak alkalis and oxidizing agents. Both PVDF and PAA can withstand the thermal treatment in this polymerization.

The pore size of PVDF membrane (Figure 3A) decreased due to the formation of PAA domain inside the pores after polymerization (Figure 3B). PAA is a non-toxic

polyelectrolyte with high ion exchange capacity. At a neutral pH, the negatively charged carboxylate ions are intended to capture the positively charged metal ions such as Fe^{2+}, which is the precursor for iron NP synthesis.[31] Based on the weight gain of membrane after polymerization and the amount of iron captured by ion exchange, the ratio of carboxyl groups and Fe^{2+} inside the membrane was calculated to be 1.8, which was close to the theoretical ratio 2. After the reduction, the core (Fe)-shell (Pd) NPs were uniformly distributed on the membrane surface (Figure 3C) and inside the pores with the size of 80 nm (Figure 3D). EDX spectrum also shows the successful coating of Pd on the surface of Fe, which adsorbed the hydrogen from iron corrosion for reduction of chlorinated organics. The particle size was dependent on the molar ratio of reducing agent ($NaBH_4$) to precursor (Fe^{2+}) during the synthesis. Thus the excessive reductant is needed to make small and uniform particles.[7] The particle loading can be increased by multi-cycle ion exchange since the carboxyl groups stay in the membranes during the NP synthesis with Na^+ as counterion.[25] However, a high loading may result in a significant increase of pressure drop through the membrane during the convective flow operation.

The water permeability reduced significantly after the Fe/Pd NP synthesis as the membrane void fraction decreased. PVDF membranes have a heterogeneous pore structure. After incorporating PAA, the membrane pore structure becomes more uniform. To study the membrane reactivity, the pores of PVDF-PAA membranes are assumed to be cylindrical for calculation purpose and PAA is uniformly distributed inside the pores (no porosity change after functionalization). The equivalent diameters d of PAA functionalized and Fe/Pd immobilized membranes can be estimated via a modified Hagen-Poisseuille equation.

$$\frac{d}{d_0}=\left(\frac{A}{A_0}\right)^{1/4} \quad (1)$$

Where d_0 and A_0 are the equivalent diameter (650 nm) and pure water permeability (4400 L/(m^2 h bar)) for PVDF membrane support, respectively. A is the pure water permeability for the pore functionalized membrane. For PVDF-PAA membrane, A is 8.38 L/(m^2 h bar) at pH=7.7, and thus d is 110 nm. For Fe/Pd immobilized membrane, A is 1.02 L/(m^2 h bar) at pH=7.5, and thus d is 80 nm. The pore size discrepancies between those calculated and observed (PVDF-PAA: 300±80 nm; PVDF-PAA-Fe/Pd: 130±50 nm from SEM images) may be due to the fracture of membrane surface during the sample preparation (liquid nitrogen treatment).

The full-scale membranes had a uniform pore size distribution and the average pore size decreased to 0.124 μm after functionalization. The ester bonds were formed between ethylene glycol and carboxyl groups (molar ratio 1:2) to prevent the leaching of PAA from the membrane.[22] These membranes were highly negatively charged based on the zeta-potential result (−46.8 mV in 1.7 mM NaCl at pH 5), showing the successful incorporation of PAA polymer in PVDF membrane pores.

3.2 Membrane responsive behavior

The polyelectrolytes with weak acid or alkali groups were reported to have a pH responsive behavior.[32–34] PAA functionalized PVDF membranes were also found to exhibit this

interesting property. Depending on the environmental pH, the carboxyl groups of PAA can be in a compact state (low pH) or an ionized state (high pH), which results in different water permeability through the membranes. The dissociation of carboxyl groups and the elongation of PAA network result in the decrease of water permeability as pH increases and passes through the pKa of PAA (4.3–4.9). Therefore, when PAA fills in PVDF membrane pores, the pore size can be tuned by varying the water pH. Hu and Dickson have studied the effects of mass gain and cross-linking degree on the pH responsive behavior of PVDF-PAA membrane.[32] They found that a lower mass gain always resulted in higher pure water permeability and a higher ratio of pure water permeability at pH 2.5 to that at 7.4. To obtain more carboxyl groups for NP synthesis while maintaining the water permeability through the pores, a monomer solution at low concentration (1.6 M) was used with a cross-linking degree of 1 mol%. 12 % mass gain was obtained after functionalization. The pure water flux through membranes at various pH values is shown in Figure 4A. The flux modulation results proved the pH reversibility of functionalized membranes. The ratio of pure water permeability at pH 3.1 to that at 7.7 was 8.6 (Figure 4B).

The pure water flux of full-scale membranes was also reproducible with pH variation (Figure 5A). The pure water permeability decreased from 1355 L/(m^2•h•bar) to 383 L/(m^2•h•bar) as the pH was increased from 3.0 to 7.3 (Figure 5B), which shows that the membrane effective pore size were highly tunable.

The full-scale membrane has a thickness of 70 μm compared to 125 μm for Millipore membrane. Its average pore size (124 nm) is also larger than that of Millipore membrane (80 nm). The pure water permeability is proportional to the reciprocal membrane thickness and the fourth power of pore size (Hagen-Poisseuille equation). Both factors result in higher pure water permeability for full-scale membrane.

3.3 PCB reductive dechlorination

The functionalized membrane support provided an opportunity to study the PCB dechlorination in both batch and convective modes. Depending on the pore size and mixing method, the resulting mass transfer could be critical in PCB dechlorination.

3.3.1 Batch reaction and NP longevity—To eliminate the effects of solvent and pH on the dechlorination rate,[35–36] all of the experiments were conducted with PCB dissolved in the deoxygenated DIUF water at pH=7.5–8.0. 2-Chlorobiphenyl was selected as the model compound due to its relatively high solubility (31.3 μM) in water. After the reduction of $NaBH_4$ and post coating of Pd, the membranes turned black and were washed with deoxygenated water until the pH of washing solution was near neutral. For each vial, two pieces of membranes were immersed into the feed solution, which gave a total loading of 0.65 g/L for Fe and 5.85 mg/L for Pd (0.9 wt% as Fe). 93 % of PCB was degraded and 91 % of biphenyl was obtained within 2 h (Figure 6). The total carbon balance was close to 95 %.

The membrane surface turned brown after dechlorination, which could be explained by the corrosion of iron with water. However, the carboxyl groups of PVDF-PAA-Fe/Pd membrane could recapture the dissolved Fe^{2+}. Otherwise, Fe^{2+} could re-precipitate on the iron surface as iron oxide. Both might take place since less than 0.6 μM of Fe (0.005 wt% of total Fe)

and 0.7 μM of Pd (1.1 wt% of total Pd) were found dissolved in the solution. The membranes were reused for dechlorination after being washed with deoxygenated water and dried under N_2 flow. The conversion of 2-chlorobiphenyl was 56 % after 2 h. The loss of reactivity could be due to the formation of iron oxide on the surface of Fe/Pd by corrosion and oxidation. Although those particles could be regenerated by the acid treatment followed by $NaBH_4$ reduction, the reactivity was at least restored partially.[37]

3.3.2 Convective flow reaction—The mass transfer resistance through a membrane barrier usually made the observed reaction rate smaller than the intrinsic rate. To obtain the intrinsic rate for 2- chlorobiphenyl dechlorination and study the stability of bimetallic NPs under the pressure, the reductive degradation was conducted under convective flow mode.

A piece of reactive membrane (6.1 mg Fe loading and 0.9 wt% Pd as Fe) was put in the dead-end filtration cell. To eliminate the loss of biphenyl product due to adsorption in the membrane domain, the biphenyl solution (26.5 μM) was first permeated through the membrane until the adsorption equilibrium (C_{feed}=$C_{permeate}$) was achieved. Then the feed solution (2-chlorobiphenyl, 31 μM) was passed through the cell. There was no biphenyl degradation with Fe/Pd NPs in the adsorption step.

The residence time of 2-chlorobiphenyl (τ) was varied by changing the pressure applied to the cell (5–11 bar). It was calculated as $\tau=V/(J_wA)$, where V is the membrane void volume ($V=\varepsilon AL$), J_w is the pure water flux at a specific pressure, A is the external area of membrane (13.2 cm^2), ε is the membrane porosity (70 %) and L is the membrane thickness (125 μm). At the neutral pH, the expanded PAA chains might overlap with each other and result in less heterogeneous pores. However, both the polymer and particles formed inside the membranes occupied some void volume. Assuming that 2- chlorobiphenyl was mainly degraded by Fe/Pd NPs inside the PAA domain when passing through pores, the membrane void volume could be obtained as $V= \varepsilon AL-V_{PAA}-V_{NP}$, where V_{PAA} is the polymer volume in the dried state (based on the weight gain of membrane after functionalization) and V_{NP} is the volume occupied by Fe/Pd NPs (calculated from the loading).

Each sample was collected after 5 min equilibration flow and one duplicate was examined to eliminate the error from catalyst deactivation. The pure water flux through the membrane was shown in Figure S1. The presence of PAA on the external surface of membrane could also cause the formation of NPs, which affected the feed concentration. Therefore, the feed concentration was analyzed throughout the reaction and the conversion was normalized. At residence times of 25.7 s, 34.6 s and 50.2 s, the conversion of PCB was 66.3 %, 74.2 % and 80.6 % respectively (Figure 7). The corresponding biphenyl yield ($[biphenyl]/[biphenyl]_{max}$) was 59.0 %, 65.1 % and 69.6 %. By increasing the residence time, the complete dechlorination could be achieved. The total carbon balance was 90 % due to the partitioning of PCB in membranes. PCB dechlroination by Fe/Pd NPs followed a pseudo-first order rate law,[8]

$$r=-\frac{dC}{dt}=k_{obs}C=k_{SA}\alpha_S\rho_m C_0(1-X) \quad (2)$$

where C_0 is the concentration of 2-chlorobiphenyl in the feed (M), C is the concentration of 2-chlorobiphenyl at the reaction time t (h), r is the reaction rate (M/h), k_{obs} is the observed rate constant (/h), k_{SA} is the surface-area-normalized rate constant (L/m^{2}h), α_s is the specific surface area of Fe/Pd NPs (m^2/g) and ρ_m is the loading of particles (58.5 g/L). If all particles were assumed to be spherical with a diameter of 80 nm and distributed uniformly, the specific surface area was 9.5 m^2/g.

As PAA and iron NPs are synthesized in PVDF membrane pores, the heterogeneity of PVDF membrane decreases and the whole membrane can be considered as a thin packed bed reactor with a uniform distribution of catalysts inside. It can be further assumed to be assembled as small packed beds. Hence, each membrane pore can be considered as a laminar flow reactor due to the small Reynolds number (Re$\ll$1). Thus,

$$X = 2\tau_0^2 \int_{\tau_0}^{\tau_\infty} \left(\frac{1}{\tau^3} - \frac{e^{-k_{obs}\tau}}{\tau^3}\right) d\tau \quad (3)$$

where X is the mean conversion of 2-chlorobiphenyl, τ_0 and τ_∞ are the residence time of 2-chlorobiphenyl at the pore center and wall (h). This equation can be solved by Hilder's approximation. Therefore, k_{SA} was 0.34, 0.33 and 0.28 L/m^{2}h at each residence time. The reaction rate under the convective flow condition ($k_{SA,average}$=0.32 L/m^{2}h) was 1.3 times higher than that in batch reaction (k_{SA}=0.26 L/m^{2}h) even though the mixing was applied. The result indicated that the convective mode operation indeed eliminated the diffusion resistance.

Fe/Pd catalyzed aqueous dechlorination (no membrane support) was also studied (Figure S2). The reaction rate obtained (0.18 L/m^{2}h) was close to the previous results (0.10–0.16 L/m^{2}h),[36] but lower than that obtained with membranes. The membrane structure could play an important role in enhancing the dechlorination by preventing the particle agglomeration. Alternatively, the cross-linker NNMA might create hydrophobic microdomains inside the polymer, which have strong affinity to hydrophobic compounds.[38] Thus PCB partitioning in the membrane was enhanced, and about 10 % of PCB in feed solution was adsorbed. For long term treatment using full-scale membrane modules, the adsorption and desorption process of PCB in the membrane may be negligible since the feed concentration is much lower (μg/L level) than that used in this study (5.9 mg/L), and the equilibrium is achieved fast with the solution recirculating through the membrane.

By increasing the Fe or Pd loading in the membrane, the dechlorinaton can also be enhanced.[22] During the NP synthesis, the carboxyl groups inside the membrane pores were deprotonated and bonded with Na^+ and then Fe^{2+} by serial ion exchange. After $NaBH_4$ reduction, the carboxyl groups were again bonded with Na^+, which indicates that the NP immobilized membranes still had the ion exchange capacity. We reported that PVDF-PAA membranes with iron oxide NPs could retain the metal ions within polymer matrix by ion exchange while maintaining the solution pH.[25] However, as the immobilized iron amount was increased by each cycle, the reduction of Fe^{2+} ion exchange was observed due to the decrease of void volume. The amount of Pd coating can also vary the reaction rate when the

Fe loading remains constant. But the percentage of reactive sites decreased when there was more than one layer of Pd on the surface of Fe.[23]

3.4 Biphenyl oxidative degradation

After the reductive dechlorination, PCB was degraded into biphenyl, which required further treatment to reduce the toxicity. Although there were studies showing that biphenyl could be decomposed by some bacteria or fungi,[39–41] the biological metabolism was a time-consuming process and usually required a moderate condition to maintain the microorganism activity. Instead, the free radical Fenton reaction was used in this study to oxidize the biphenyl.

Fe NPs were partially oxidized after the reaction due to the water corrosion. Thus a layer of iron oxides was found deposited on the surface of Fe/Pd.[23] In the presence of iron oxides, OH• are generated in H_2O_2 decomposition, and able to oxidize most recalcitrant organics at near diffusion-controlled rates. On the other hand, Fe NPs which were not oxidized in the dechlorination can also react with H_2O_2, producing OH•. Both dissolved Fe^{2+} and highly reactive iron oxide formed in iron oxidation with H_2O_2 can enhance the free radical generation.[42]

The reactivity of membranes with Fe/Pd (after dechlorination), Fe (freshly made) and iron oxide NPs (synthesized via air oxidation of Fe)[25] in biphenyl oxidation were compared by adding the same amount of H_2O_2 (10 mM) in each system. The temperature of solution increased 3 °C after the H_2O_2 addition. Biphenyl was completely degraded within 15 min by Fe/Pd or Fe immobilized membranes (Figure 8A). pH dropped significantly, and less than 70 μM of Fe (0.6 wt% of total Fe) and 2.3 μM of Pd (4.2 wt% of total Pd) were found dissolved in the solution. It was also observed that Fe/Pd utilized more H_2O_2 than Fe (Figure 8B), which could be explained by hydrogenation and/or decomposition of H_2O_2 to water by Pd catalyst.[43] However, Pd was not necessary in this oxidative step. Iron oxide reacted with H_2O_2 relatively slowly, and the oxidation of model compound was highly dependent on the regeneration of Fe (II) from Fe (III).[12] But it might give a higher overall H_2O_2 efficiency, which was defined as $\Delta[\text{model compound}]/\Delta[H_2O_2]$.

3.5 Intermediate and product analysis

The direct products in radiolytic oxidation of biphenyl by OH• were hydroxylated biphenyls including 2-, 3- and 4-hydroxybiphenyl.[44] These intermediates could be further oxidized by OH•, forming the secondary products such as dihydroxybiphenyls. Sedlak and Andren detected hydroxychlorobiphenyls and dihydroxylated chlorobiphenyls in aqueous oxidation of 2-chlorobiphenyl by Fenton reaction.[18] Li et al. reported that biphenyl was successfully oxidized by OH• in chelate-modified Fenton reaction. Several intermediates were determined including the aromatic ring cleavage products such as benzoic acid and hydroxybenzoic acid.[45] Therefore, the biphenyl oxidation started with the hydroxylation of aromatic rings, followed by the ring cleavage. If enough oxidants are provided, the carboxylic acids or even carbon dioxide are expected to be obtained. However, that may not be cost-effective or necessary.

The phenolic compounds usually have low response in GC due to their polarity. The derivatizing agent converts the -OH groups to nonpolar and more volatile groups, allowing the GC analysis. The hexane used to extract the samples was evaporated under gentle N_2 flow followed by the addition of BSTFA/Pyridine. The three peaks shown in Figure 9C represented 2-, 3- and 4-hydroxybiphenyl (Figure S3), respectively. 2,2'-Dihydroxybiphenyl (Figure S4) and benzoic acid (Figure S5) were also identified. However, the existence of more polar products (such as small organic acids[46]) from ring cleavage was not disproven since they might not be amenable to the solvent extraction and/or GC/MS analysis used in this study. Another four dihydroxybiphenyls and eight trihydroxybiphenyls (Figure S6) were tentatively identified (without standard) based on their mass spectra. These results are consistent with the findings of Halpaap et al..[47] They reported the existence of mono-, di- and trihydroxybiphenyl products during the metabolism of biphenyl in the rat, which were mainly due to the oxidative stress in rat body.

The intermediates detected were all more soluble than biphenyl. Therefore, they might compete with biphenyl to react with OH•. Thus only a small amount existed in the solution. On the other hand, the iron oxidation with H_2O_2 produced the free radicals very efficiently, which might destroy the biphenyl and its oxidation products instantly. To understand the evolution of intermediates during the oxidation, 2-hydroxybiphenyl (0.431 mM), one of the direct products in biphenyl oxidation, were used as the model compound in iron oxide/H_2O_2 system. The iron oxide catalyzed free radical reaction can be described as a second order reaction[48] and thus Equation 4 was obtained.

$$-\frac{dC_{2OHBP}}{dt}=kC_{2OHBP}C_{OH\bullet} \quad (4)$$

Where C_{2OHBP} is the concentration of 2-hydroxybiphenyl in the solution, C_{OH}• is the concentration of OH• and k is the second order rate constant. Since H_2O_2 was maintained at a constant concentration, a pseudo-first order reaction model could be obtained.

$$-\frac{dC_{2OHBP}}{dt}=k'C_{2OHBP} \quad (5)$$

Where $k'=kC_{OH}$•. As shown in Figure 10, the oxidation of 2-hydroxybiphenyl fit the pseudo-first order approximation well (R^2=0.96).

The samples were analyzed with the same protocol and the peak areas of different components were compared. For most compounds, the peak areas increased first, and then maintained constant. This trend again shows that the hydroxylated biphenyls and benzoic acid were indeed the reaction products. Further study will focus on the intermediate quantification.

3.6 Oxidation mechanism

Both Fe/Pd and Fe NPs show high reactivity with H_2O_2 in OH• generation during the biphenyl oxidation. A significant pH drop was observed due to the increase of dissolved Fe^{2+} during the oxidation. Similar results were reported in the degradation of bromothymol blue and methyl tert-butyl ether (MTBE),[49–50] in which Fe^{2+} was generated at acidic

condition (pH=4–7) via iron oxidation with H_2O_2 (Equation 6), and enhanced the OH• generation in a Fenton-like mechanism.

$$Fe + H_2O_2 \rightarrow Fe^{2+} + 2OH^- \quad (6)$$

$$Fe^{2+} + H_2O_2 \rightarrow Fe^{3+} + OH\bullet + OH^- \quad (7)$$

$$Fe(II) + H_2O_2 \rightarrow Fe(III) + OH\bullet + OH^- \quad (8)$$

Equation 7 is the Fenton reaction in the aqueous phase. As Fe^{2+} released from the Fe surface precipitated as iron oxide (II, III), a similar electron transfer was initiated on the iron oxide surface (Equation 8). The iron oxide catalytic centers were found even more effective in the production of OH• than dissolved iron (Fe^{2+}, Fe^{3+}).[49, 51] A similar system was iron NPs with oxygen-containing water, in which H_2O_2 was provided via the iron oxidation and the contaminants were degraded by oxidative transformation.[29, 42]

To study the iron/iron oxide transformation during H_2O_2 oxidation, multi-cycle of H_2O_2 was added into the freshly made Fe NP solution under the anaerobic condition (by N_2 purging), while the oxidative transformation of NPs were monitored using XRD. For the freshly made iron, H_2O_2 was consumed instantly due to the formation of Fe^{2+}/Fe (II). As iron was oxidized, the reaction rate decreased and became like a pseudo-first order rate usually observed in heterogeneous Fenton reaction (Figure 11A). Therefore, iron oxide must be formed on the iron surface. The XRD spectrum of iron before and after H_2O_2 treatment (Figure 11B) further proved it. The body-centered cubic α-Fe (Figure 11B, a) was mainly converted into magnetite Fe_3O_4 (Figure 11B, b), which is one of most reactive iron oxides known in nature.[11, 52] By utilizing the STEM-EELS (line scan and elemental mapping), the morphology and composition change of Fe NPs during the H_2O_2 oxidation were visualized. It was observed that even for fresh Fe NPs there was an oxide shell about 3–5 nm (Figure 12A), which was consistent with previous results.[53] After the first cycle, the thickness of oxide layer was increased to 20–30 nm (Figure 12B), and the oxide formed had an amorphous structure, which was mainly nanoscale magnetite agglomerate based on the XRD result. At the end of six cycle treatment, the particles were completely oxidized (Figure 12C) and it was hard to differentiate the iron core from the surrounded iron oxide shell. This indicated that H_2O_2 treatment resulted in the transformation from iron to magnetite under the anaerobic condition. The oxidation of iron NPs slows down the production of free radicals, but iron oxide NPs formed can still perform as the heterogeneous Fenton catalyst for a long time.[11,16, 25] The efficiency to generate free radicals by iron oxide NPs is reduced by the continuous addition of H_2O_2.[25] The reactivity of iron/iron oxide NPs can be enhanced by either reduction (with acid treatment) or loading the fresh particles. For a full-scale process, the membrane modules with exhausted catalysts can be replaced by new modules or regenerated by first dissolving the iron oxide followed by ion exchange (Fe^{2+}) and reduction.

3.8 Applications

Iron/iron oxide embedded microfiltration membrane modules have the potential to enhance the overall degradation efficiency of contaminant water with a combined reductive and oxidative treatment. In real life treatment, PCBs are reduced to biphenyl when passing through the first module (PVDF-PAA-Fe/Pd), followed by mixing with H_2O_2 and subsequent oxidation in the second module (PVDF-PAA-Fe or Fe_xO_y). Each module is accompanied by a recirculating device to achieve high conversions. H_2O_2 can be continuously supplied by another module with enzyme (glucose oxidase) immobilization (layer-by-layer assembly).[3] This reactive membrane platform enhances the reactivity of NPs (no agglomeration) while eliminating the formation of chlorinated byproducts in the direct oxidation with Fe^{2+} or iron oxide immobilized membranes.[31]

4. Conclusions

This study has demonstrated that the complete degradation of PCBs can be achieved via a combined reductive/oxidative pathway, using reactive membranes incorporated with iron related NPs (Fe, Fe/Pd, iron oxide). The PAA functionalized PVDF membranes provided a tunable platform for NP synthesis. By using Fe/Pd embedded membranes, 2- chlorobiphenyl was successfully converted into biphenyl. In the batch reaction, the functionalized membrane support prevented the agglomeration of NPs and enhanced the reactivity by 1.4 times (k_{SA}: 0.18→0.26 L/m^{2}h). Under the convective mode, the mass transfer resistance was effectively eliminated and the rate constant was increased by 1.3 times (k_{SA}: 0.26→0.32 L/m^{2}h) compared with the batch study result. Mono-, di- and trihydroxybiphenyls and benzoic acid were detected as the main products in the subsequent oxidation of biphenyl by OH•. Thus the oxidation started with the hydroxylation of aromatic ring followed by the ring cleavage. The dissolved Fe^{2+} and iron oxide (magnetite) on the Fe surface both enhanced the oxidative dechlorination. Our recent development in full-scale membrane functionalization proved the possibility of using this platform for the practical water remediation.

Supplementary Material

Refer to Web version on PubMed Central for supplementary material.

Acknowledgments

This study was supported by the National Institute of Environmental Health Sciences Superfund Research (NIEHS-SRP) program (P42ES007380) and by the Department of Energy DOE-KRCEE program (DE-FG05-03OR23032). We thank Dr. Jia Ye from the Electron Microscopy Center (University of Kentucky) for STEM-EELS mapping analytical support, and John May from Environmental Research and Training Laboratory (ERTL) at UK for GC-MS analytical assistance. The authors acknowledge the highly significant contributions of Sepro Membrane Co. of Oceanside, CA towards the joint development of full-scale PVDF functionalized membranes.

References

1. Dai JH, Bruening ML. Catalytic nanoparticles formed by reduction of metal ions in multilayered polyelectrolyte films. Nano Lett. 2002; 2:497–501.
2. Ulbricht M. Advanced functional polymer membranes. Polymer. 2006; 47:2217–2262.

3. Datta S, Cecil C, Bhattacharyya D. Functionalized membranes by layer-by-layer assembly of polyelectrolytes and in situ polymerization of acrylic acid for applications in enzymatic catalysis. Ind. Eng. Chem. Res. 2008; 47:4586–4597.
4. Kim J, Van der Bruggen B. The use of nanoparticles in polymeric and ceramic membrane structures: Review of manufacturing procedures and performance improvement for water treatment. Environ. Pollut. 2010; 158:2335–2349. [PubMed: 20430495]
5. Johnson TL, Scherer MM, Tratnyek PG. Kinetics of halogenated organic compound degradation by iron metal. Environ. Sci. Technol. 1996; 30:2634–2640.
6. Wang CB, Zhang WX. Synthesizing nanoscale iron particles for rapid and complete dechlorination of TCE and PCBs. Environ. Sci. Technol. 1997; 31:2154–2156.
7. Zhang WX. Nanoscale iron particles for environmental remediation: An overview. J. Nanopart. Res. 2003; 5:323–332.
8. Lien HL, Zhang WX. Nanoscale Pd/Fe bimetallic particles: Catalytic effects of palladium on hydrodechlorination. Appl. Catal. B-Environ. 2007; 77:110–116.
9. He F, Zhao DY. Hydrodechlorination of trichloroethene using stabilized Fe-Pd nanoparticles: Reaction mechanism and effects of stabilizers, catalysts and reaction conditions. Appl. Catal. B-Environ. 2008; 84:533–540.
10. Tee YH, Bachas L, Bhattacharyya D. Degradation of trichloroethylene and dichlorobiphenyls by iron-based bimetallic nanoparticles. J. Phys. Chem. C. 2009; 113:9454–9464.
11. Watts RJ, Udell MD, Kong SH, Leung SW. Fenton-like soil remediation catalyzed by naturally occurring iron minerals. Environ. Eng. Sci. 1999; 16:93–103.
12. Pignatello JJ, Oliveros E, MacKay A. Advanced oxidation processes for organic contaminant destruction based on the Fenton reaction and related chemistry. Crit. Rev. Env. Sci. Tec. 2006; 36:1–84.
13. Zelmanov G, Semiat R. Iron(3) oxide-based nanoparticles as catalysts in advanced organic aqueous oxidation. Water Res. 2008; 42:492–498. [PubMed: 17714754]
14. Costa RCC, Moura FCC, Ardisson JD, Fabris JD, Lago RM. Highly active heterogeneous Fenton-like systems based on Fe^0/Fe_3O_4 composites prepared by controlled reduction of iron oxides. Appl. Catal. B-Environ. 2008; 83:131–139.
15. Pham ALT, Lee C, Doyle FM, Sedlak DL. A silica-supported iron oxide catalyst capable of activating hydrogen peroxide at neutral pH values. Environ. Sci. Technol. 2009; 43:8930–8935. [PubMed: 19943668]
16. Sun SP, Lemley AT. p-Nitrophenol degradation by a heterogeneous Fenton-like reaction on nano-magnetite: Process optimization, kinetics, and degradation pathways. J. Mol. Catal. A-Chem. 2011; 349:71–79.
17. Lowry GV, Johnson KM. Congener-specific dechlorination of dissolved PCBs by microscale and nanoscale zerovalent iron in a water/methanol solution. Environ. Sci. Technol. 2004; 38:5208–5216. [PubMed: 15506219]
18. Sedlak DL, Andren AW. Aqueous-phase oxidation of polychlorinated-biphenyls by hydroxyl radicals. Environ. Sci. Technol. 1991; 25:1419–1427.
19. Pignatello JJ, Chapa G. Degradation of PCBs by ferric ion, hydrogen peroxide and UV Light. Environ. Toxicol. Chem. 1994; 13:423–427.
20. Ahmad M, Simon MA, Sherrin A, Tuccillo ME, Ullman JL, Teel AL, Watts RJ. Treatment of polychlorinated biphenyls in two surface soils using catalyzed H_2O_2 propagations. Chemosphere. 2011; 84:855–862. [PubMed: 21733547]
21. Smuleac V, Varma R, Sikdar S, Bhattacharyya D. Green synthesis of Fe and Fe/Pd bimetallic nanoparticles in membranes for reductive degradation of chlorinated organics. J. Membrane Sci. 2011; 379:131–137.
22. Smuleac V, Bachas L, Bhattacharyya D. Aqueous-phase synthesis of PAA in PVDF membrane pores for nanoparticle synthesis and dichlorobiphenyl degradation. J. Membrane Sci. 2010; 346:310–317.
23. Xu J, Bhattacharyya D. Fe/Pd nanoparticle immobilization in microfiltration membrane pores: Synthesis, characterization, and application in the dechlorination of polychlorinated biphenyls. Ind. Eng. Chem. Res. 2007; 46:2348–2359.

24. Xu J, Dozier A, Bhattacharyya D. Synthesis of nanoscale bimetallic particles in polyelectrolyte membrane matrix for reductive transformation of halogenated organic compounds. J. Nanopart. Res. 2005; 7:449–467.
25. Gui MH, Smuleac V, Ormsbee LE, Sedlak DL, Bhattacharyya D. Iron oxide nanoparticle synthesis in aqueous and membrane systems for oxidative degradation of trichloroethylene from water. J. Nanopart. Res. 2012; 14:861.
26. Wang XY, Chen C, Liu HL, Ma J. Preparation and characterization of PAA/PVDF membrane-immobilized Pd/Fe nanoparticles for dechlorination of trichloroacetic acid. Water Res. 2008; 42:4656–4664. [PubMed: 18775551]
27. Wu LF, Ritchie SM. C. Enhanced dechlorination of trichloroethylene by membrane-supported Pd-coated iron nanoparticles. Environ. Prog. 2008; 27:218–224.
28. Lewis S, Smuleac V, Montague A, Bachas L, Bhattacharyya D. Iron-functionalized membranes for nanoparticle synthesis and reactions. Separ. Sci. Technol. 2009; 44:3289–3311.
29. Joo SH, Feitz AJ, Waite TD. Oxidative degradation of the carbothioate herbicide, molinate, using nanoscale zero-valent iron. Environ. Sci. Technol. 2004; 38:2242–2247. [PubMed: 15112830]
30. Clapp PA, Evans DF, Sheriff TS. S. Spectrophotometric determination of hydrogen peroxide after extraction with ethyl-acetate. Anal. Chim. Acta. 1989; 218:331–334.
31. Lewis SR, Datta S, Gui M, Coker EL, Huggins FE, Daunert S, Bachas L, Bhattacharyya D. Reactive nanostructured membranes for water purification. Proc. Natl. Acad. Sci. U S A. 2011; 108:8577–82. [PubMed: 21606340]
32. Hu K, Dickson JM. Development and characterization of poly(vinylidene fluoride)-poly (acrylic acid) pore-filled pH-sensitive membranes. J. Membrane Sci. 2007; 301:19–28.
33. Wandera D, Wickramasinghe SR, Husson SM. Stimuli-responsive membranes. J. Membrane Sci. 2010; 357:6–35.
34. Stuart MAC, Huck WTS, Genzer J, Muller M, Ober C, Stamm M, Sukhorukov GB, Szleifer I, Tsukruk VV, Urban M, Winnik F, Zauscher S, Luzinov I, Minko S. Emerging applications of stimuli-responsive polymer materials. Nat. Mater. 2010; 9:101–113. [PubMed: 20094081]
35. Fang Y, Al-Abed SR. Correlation of 2-chlorobiphenyl dechlorination by Fe/Pd with iron corrosion at different pH. Environ. Sci. Technol. 2008; 42:6942–6948. [PubMed: 18853813]
36. Fang YX, Al-Abed SR. Dechlorination kinetics of monochlorobiphenyls by Fe/Pd: Effects of solvent, temperature, and PCB concentration. Appl. Catal. B-Environ. 2008; 78:371–380.
37. Zhu BW, Lim TT. Catalytic reduction of chlorobenzenes with Pd/Fe nanoparticles: reactive sites, catalyst stability, particle aging, and regeneration. Environ. Sci. Technol. 2007; 41:7523–7529. [PubMed: 18044536]
38. Wang GJ, Engberts JBFN. Synthesis and catalytic properties of cross-linked hydrophobically associating poly(alkylmethyldiallylammonium bromides). J. Org. Chem. 1994; 59:4076–4081.
39. Schwartz RD, Williams AL, Hutchinson DB. Microbial production of 4,4'- dihydroxybiphenyl: biphenyl hydroxylation by fungi. Appl. Environ. Microb. 1980; 39:702–708.
40. Yang S, Yoshida N, Baba D, Katayama A. Anaerobic biodegradation of biphenyl in various paddy soils and river sediment. Chemosphere. 2008; 71:328–336. [PubMed: 17950776]
41. Mohn WW, Westerberg K, Cullen WR, Reimer KJ. Aerobic biodegradation of biphenyl and polychlorinated biphenyls by arctic soil microorganisms. Appl. Environ. Microb. 1997; 63:3378–3384.
42. Keenan CR, Sedlak DL. Factors affecting the yield of oxidants from the reaction of manoparticulate zero-valent iron and oxygen. Environ. Sci. Technol. 2008; 42:1262–1267. [PubMed: 18351103]
43. Okada S, Mori K, Kamegawa T, Che M, Yamashita H. Active site design in a core-shell nanostructured catalyst for a one-pot oxidation reaction. Chem-Eur. J. 2011; 17:9047–9051. [PubMed: 21744408]
44. Chen XF, Schuler RH. Directing effects of phenyl substitution in the reaction of hydroxyl radical with aromatics: the radiolytic hydroxylation of biphenyl. J. Phys. Chem.-Us. 1993; 97:421–425.
45. Li YC, Bachas LG, Bhattacharyya D. Selected chloro-organic detoxifications by polychelate (poly(acrylic acid)) and citrate-based Fenton reaction at neutral pH environment. Ind. Eng. Chem. Res. 2007; 46:7984–7992.

46. Li, YC. Detoxification of selected chloro-organics by oxidation technique Using chelate modified Fenton reaction. PhD. Dissertation. Lexington, KY: University of Kentucky; 2007.
47. Halpaap K, Horning MG, Horning EC. Metabolism of biphenyl in the rat. J. Chromatogr. 1978; 166:479–490. [PubMed: 748358]
48. Valentine RL, Wang HCA. Iron oxide surface catalyzed oxidation of quinoline by hydrogen peroxide. J. Environ. Eng.-Asce. 1998; 124:31–38.
49. Bergendahl JA, Thies TP. Fenton's oxidation of MTBE with zero-valent iron. Water Res. 2004; 38:327–334. [PubMed: 14675644]
50. Hoag GE, Collins JB, Holcomb JL, Hoag JR, Nadagouda MN, Varma RS. Degradation of bromothymol blue by 'greener' nano-scale zero-valent iron synthesized using tea polyphenols. J. Mater. Chem. 2009; 19:8671–8677.
51. Voinov MA, Pagan JOS, Morrison E, Smirnova TI, Smirnov AI. Surface-mediated production of hydroxyl radicals as a mechanism of iron oxide nanoparticle biotoxicity. J Am. Chem. Soc. 2011; 133:35–41. [PubMed: 21141957]
52. Tyre BW, Watts RJ, Miller GC. Treatment of four biorefractory contaminants in soils using catalyzed hydrogen peroxide. J. Environ. Qual. 1991; 20:832–838.
53. Nurmi JT, Tratnyek PG, Sarathy V, Baer DR, Amonette JE, Pecher K, Wang CM, Linehan JC, Matson DW, Penn RL, Driessen MD. Characterization and properties of metallic iron nanoparticles: Spectroscopy, electrochemistry, and kinetics. Environ. Sci. Technol. 2005; 39:1221–1230. [PubMed: 15787360]

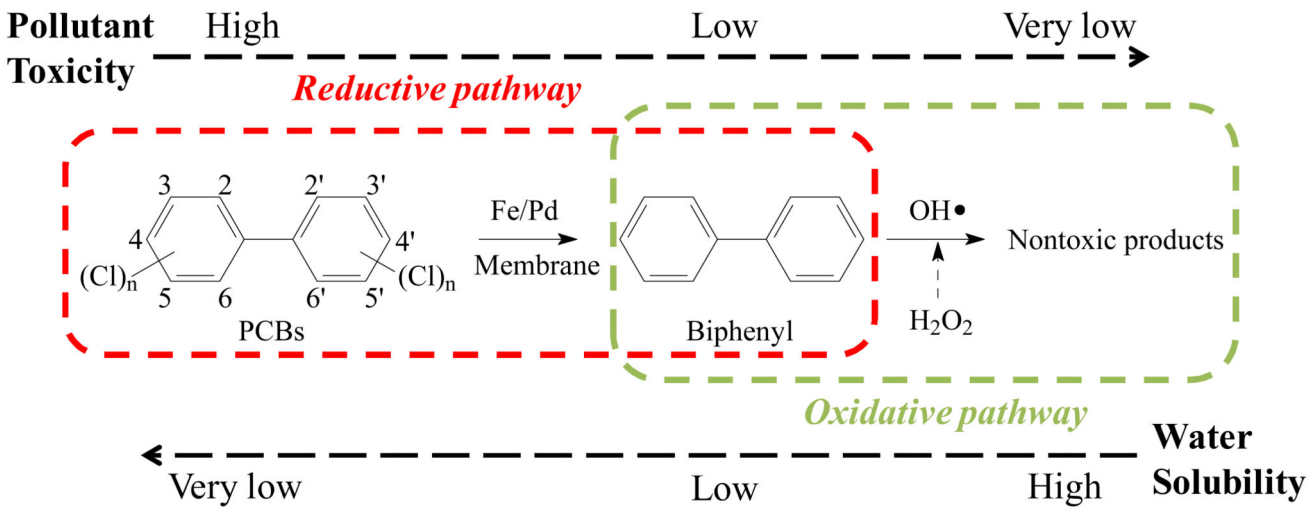

Figure 1.
The combined (reductive and oxidative) pathway for PCB detoxification.

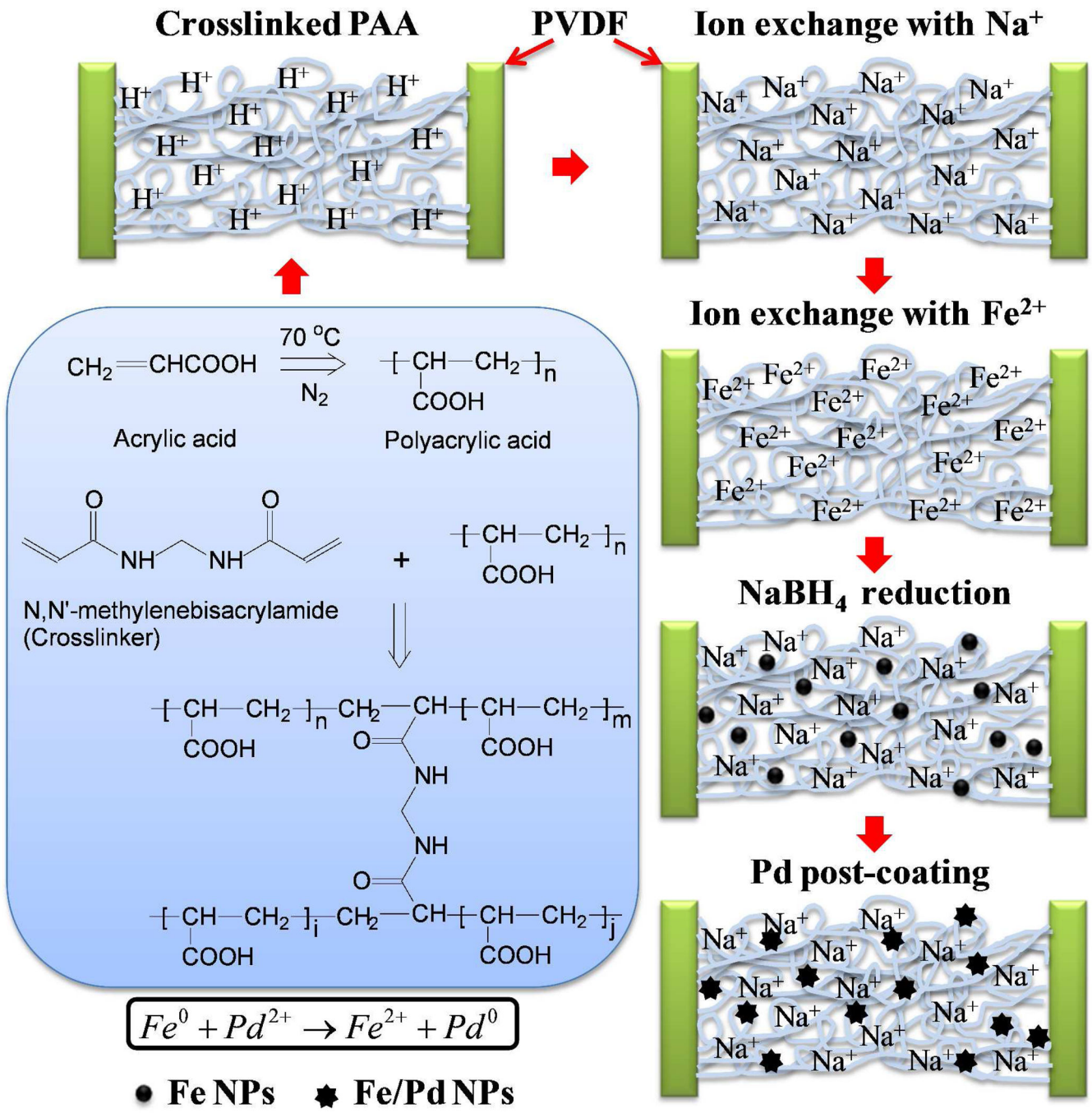

Figure 2.
PVDF membrane pore functionalization by in-situ polymerization of acrylic acid (AA) and synthesis of Fe/Pd bimetallic NPs inside the pores.

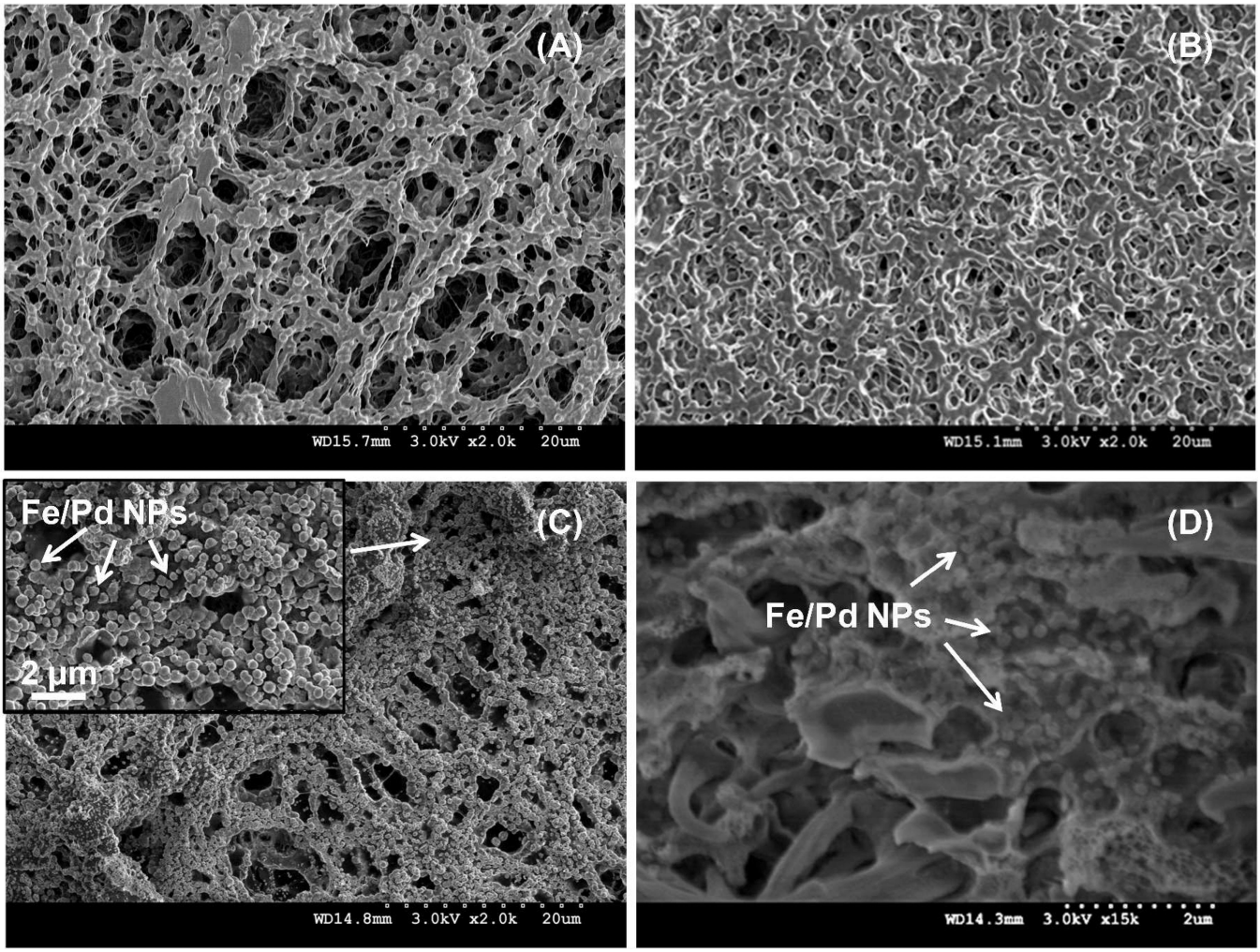

Figure 3.

SEM image of Millipore PVDF (A), PVDF-PAA (B) and Fe/Pd immobilized PVDF-PAA membrane surface (C) and cross-section (D). White arrows indicate the Fe/Pd NPs.

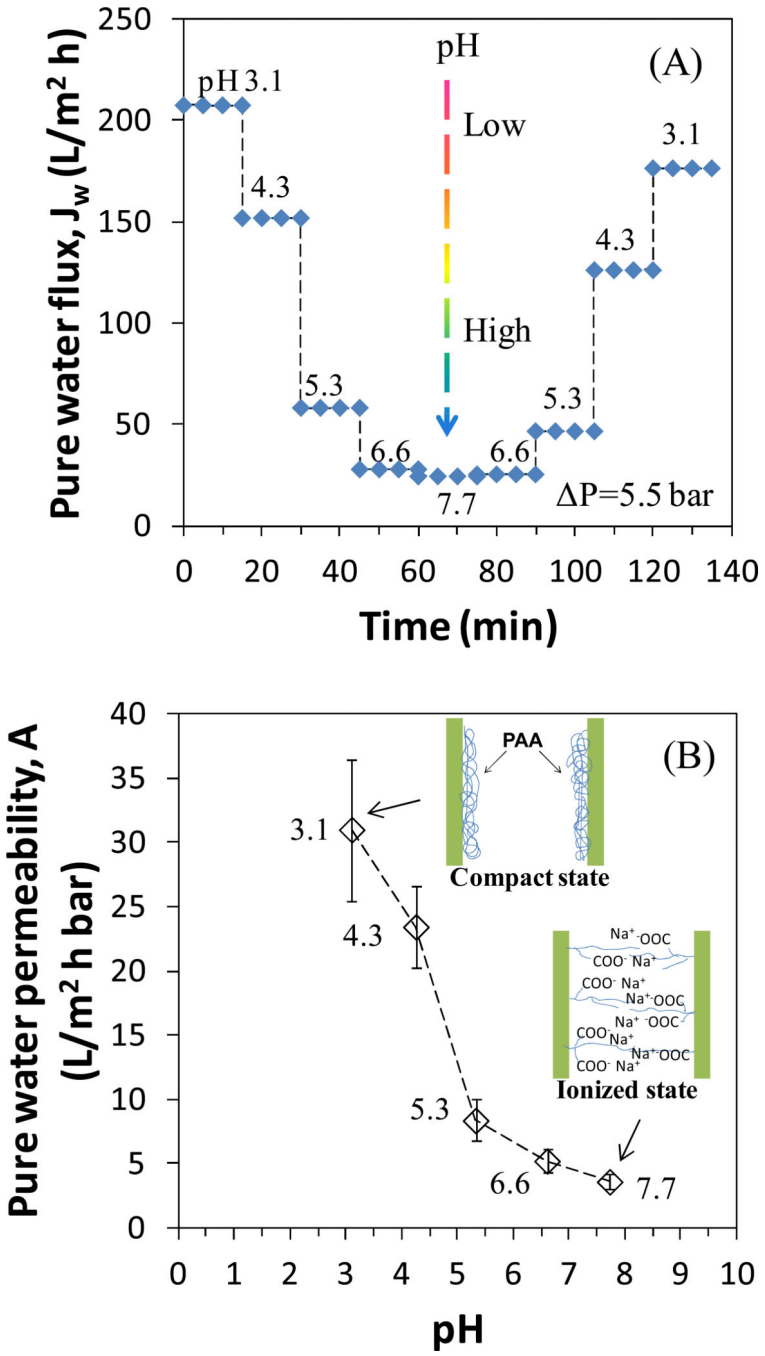

Figure 4.

Flux modulation of bench-scale PVDF-PAA membranes by pH. (A) Pure water flux at 5.5 bar and (B) pure water permeability. At each pH, three samples were collected after the permeate pH became the same as the feed. Thickness of PVDF membranes: 125 μm.

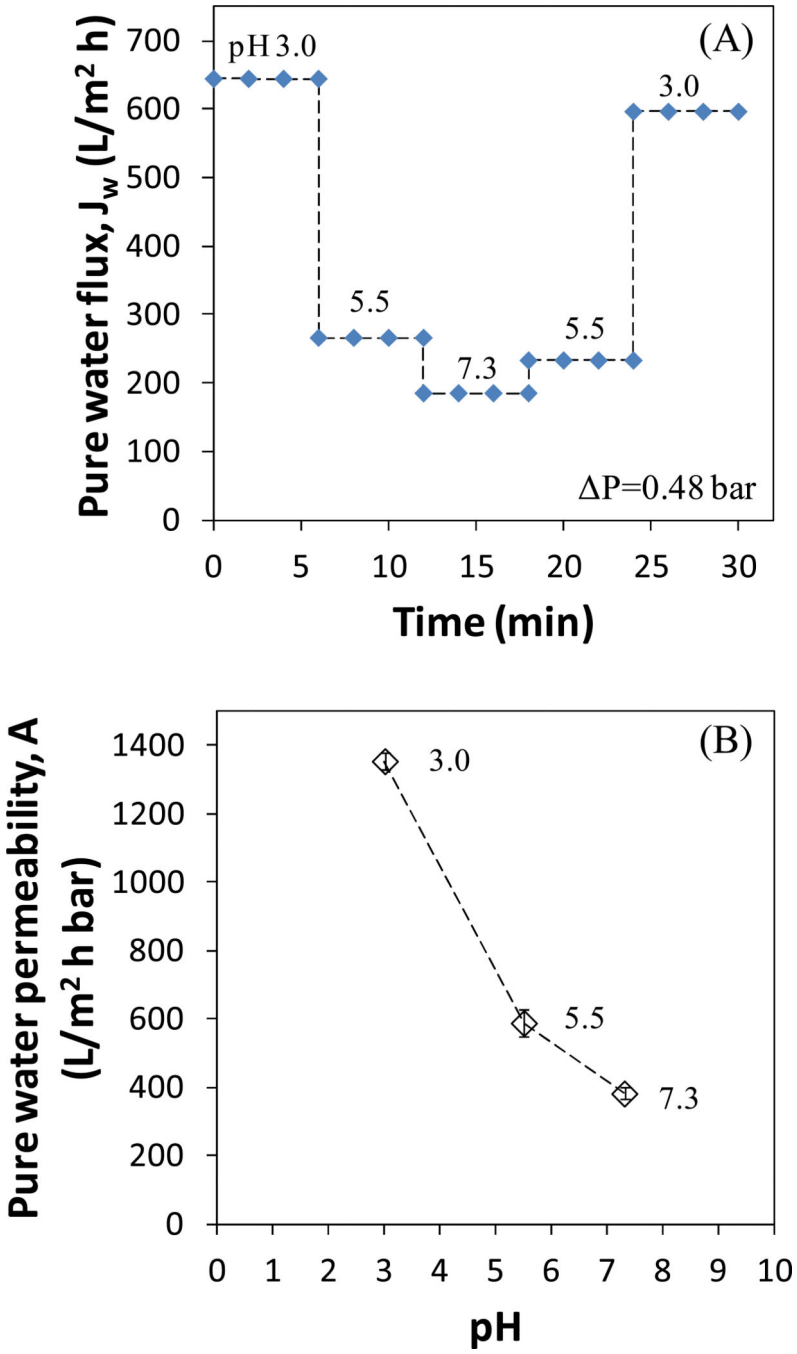

Figure 5.

Flux modulation of full-scale PVDF-PAA membranes by pH. (A) Pure water flux at 0.48 bar and (B) pure water permeability. At each pH, three samples were collected after the permeate pH became the same as the feed. Thickness of PVDF layer: 70 μm.

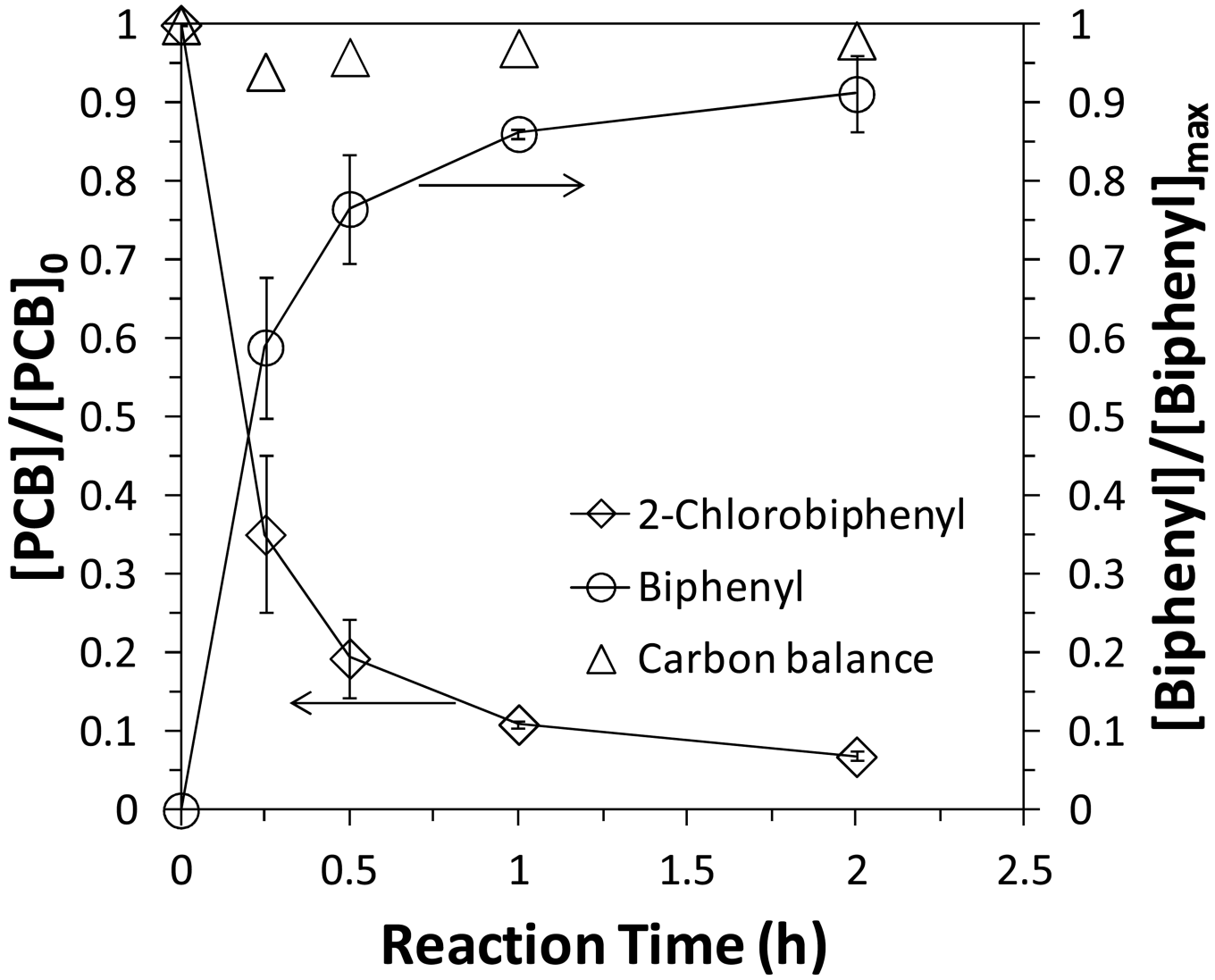

Figure 6.

Batch study (no convective flow through the pores) of PCB (2-chlorobiphenyl) dechlorination and biphenyl formation by Fe/Pd NP immobilized PVDF-PAA membranes. $[PCB]_0$=31μM, [Fe]=0.65 g/L (size: 80 nm), [Pd]=0.9 wt% as Fe, pH=7.5– 8.0.

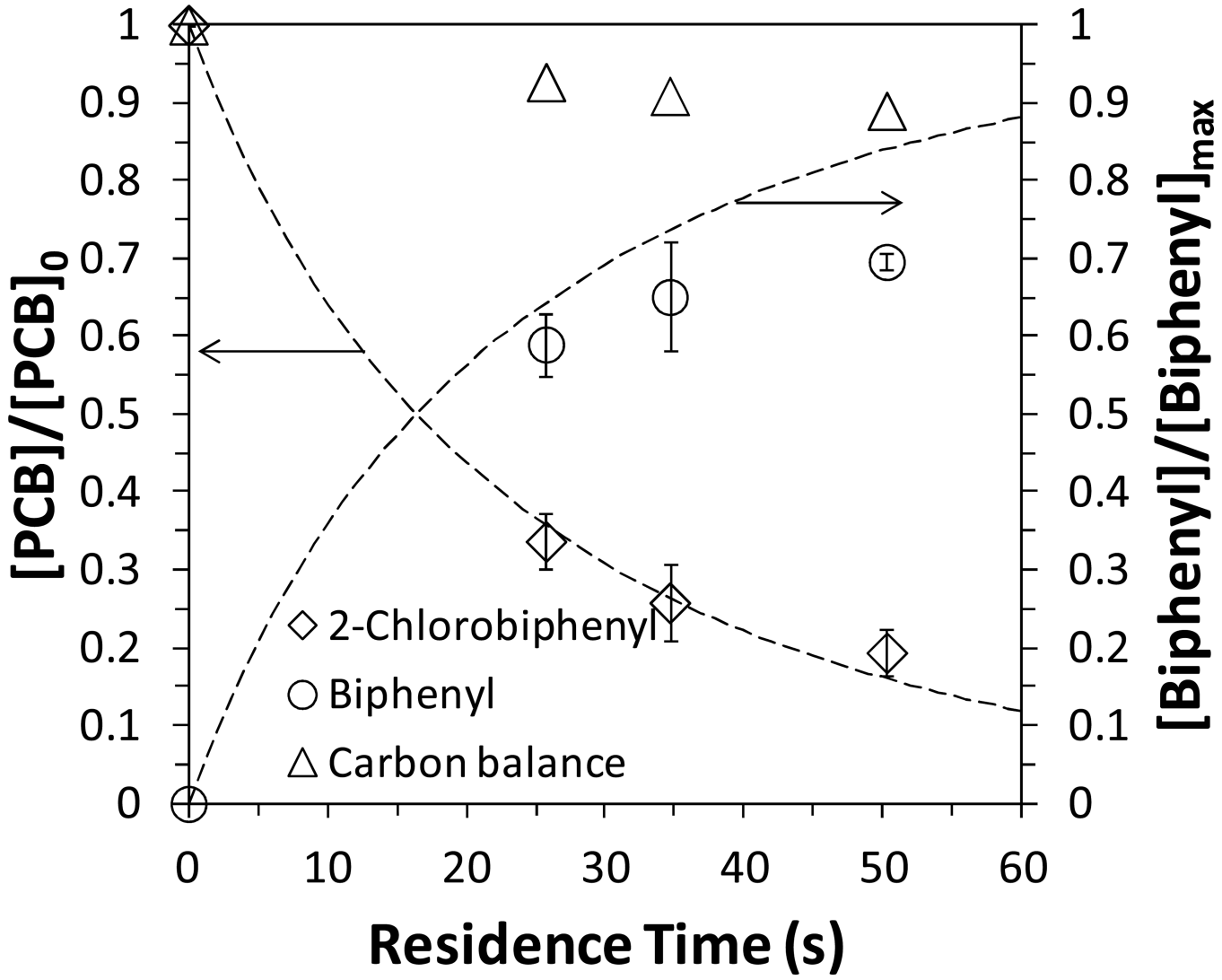

Figure 7.

Convective flow study of PCB (2-chlorobiphenyl) dechlorination and biphenyl formation by Fe/Pd NP immobilized PVDF-PAA membranes. $[PCB]_0$=31μM, mass (Fe)=6.1 mg (size: 80 nm, ρ_m=58.5 g/L), [Pd]=0.9 wt% as Fe, pH=7.5–8.0. Pressure varied between 5 and 11 bar. Membrane external area: 13.2 cm^2. Dash lines are the 2-chlorobiphenyl and biphenyl concentration predicted using laminar flow reactor model and the average k_{SA} obtained (0.32 L/m^2h).

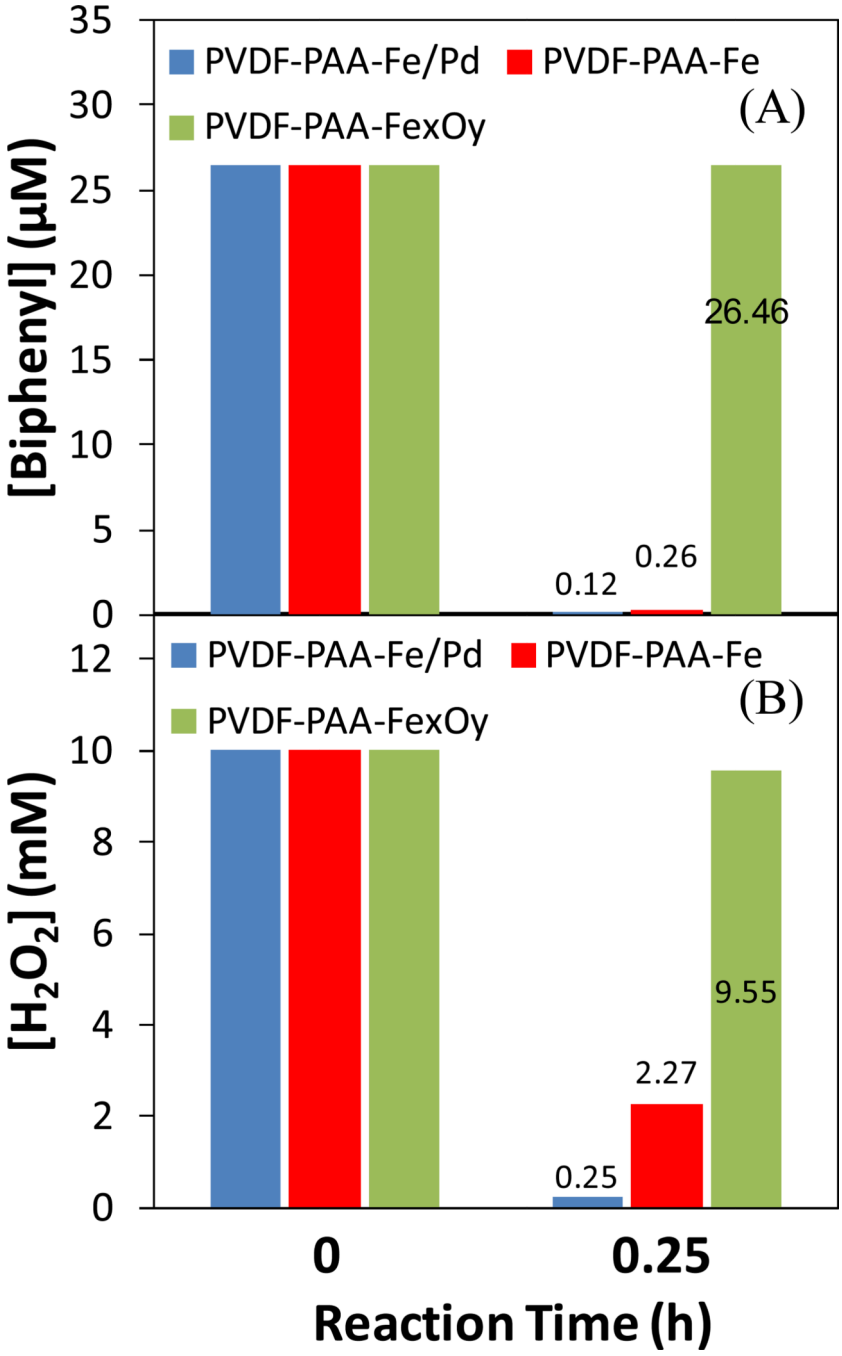

Figure 8.

Batch study of (A) biphenyl oxidation and (B) H_2O_2 consumption with Fe/Pd, Fe and Fe_xO_y (iron oxide) immobilized PVDF-PAA membranes. $[Biphenyl]_0$=26.5 μM, $[H_2O_2]_2$=10 mM, [Fe]=0.65 g/L, [Pd]=0.9 wt% as Fe. pH changes during the reaction: PVDF-PAA-Fe/Pd (7.2→4.0), PVDF-PAA-Fe (6.6 →5.0), PVDF-PAA-iron oxide (6.6 →6.5).

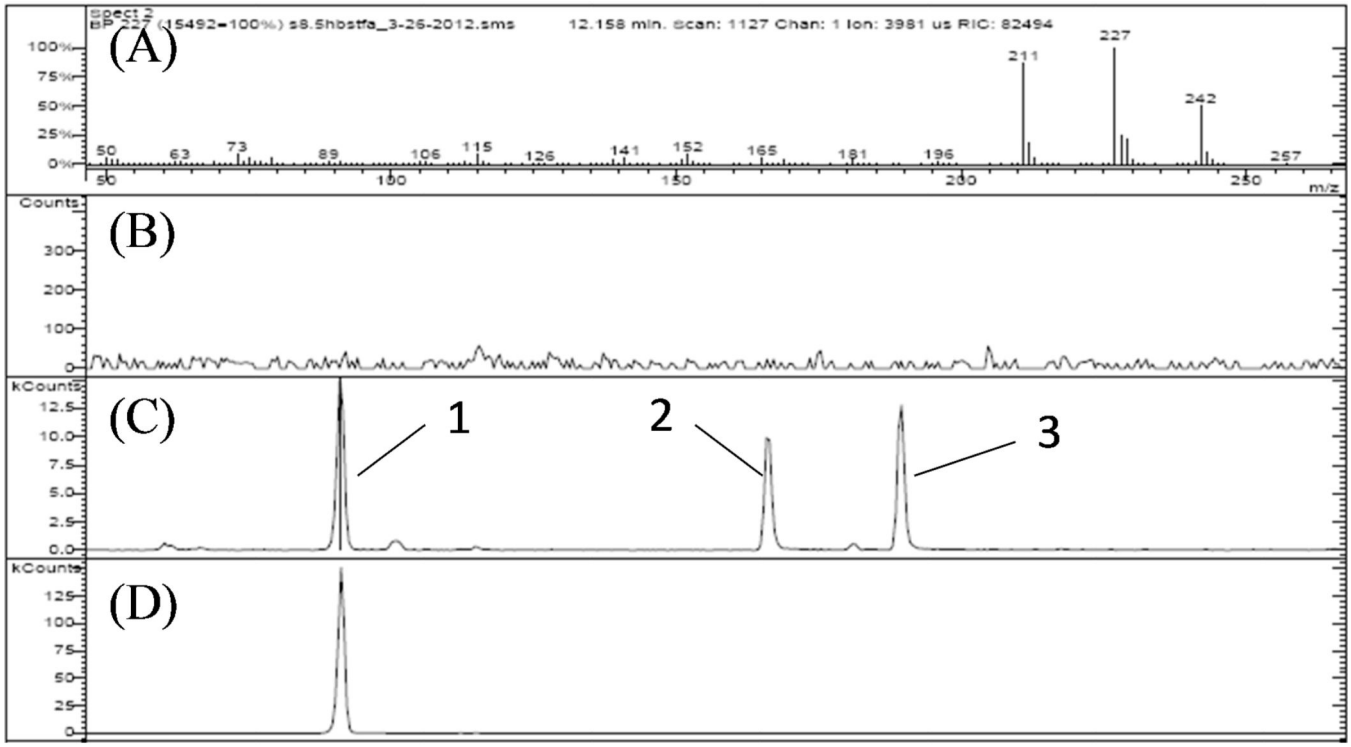

Figure 9.

2-Hydroxybiphenyl (BSTFA derivatized) detected in biphenyl oxidation by Fe/Pd NP immobilized PVDF-PAA membranes (peak 1). (A) Mass spectrum (Selected ion: 227); (B) Chromatograph of BSTFA/Pyridine; (C) Chromatograph of sample; (D) Chromatograph of 2-hydroxybiphenyl standard. Peak 2 and 3 indicate 3- and 4- hydroxybiphenyl, respectively (see supporting information Figure S2).

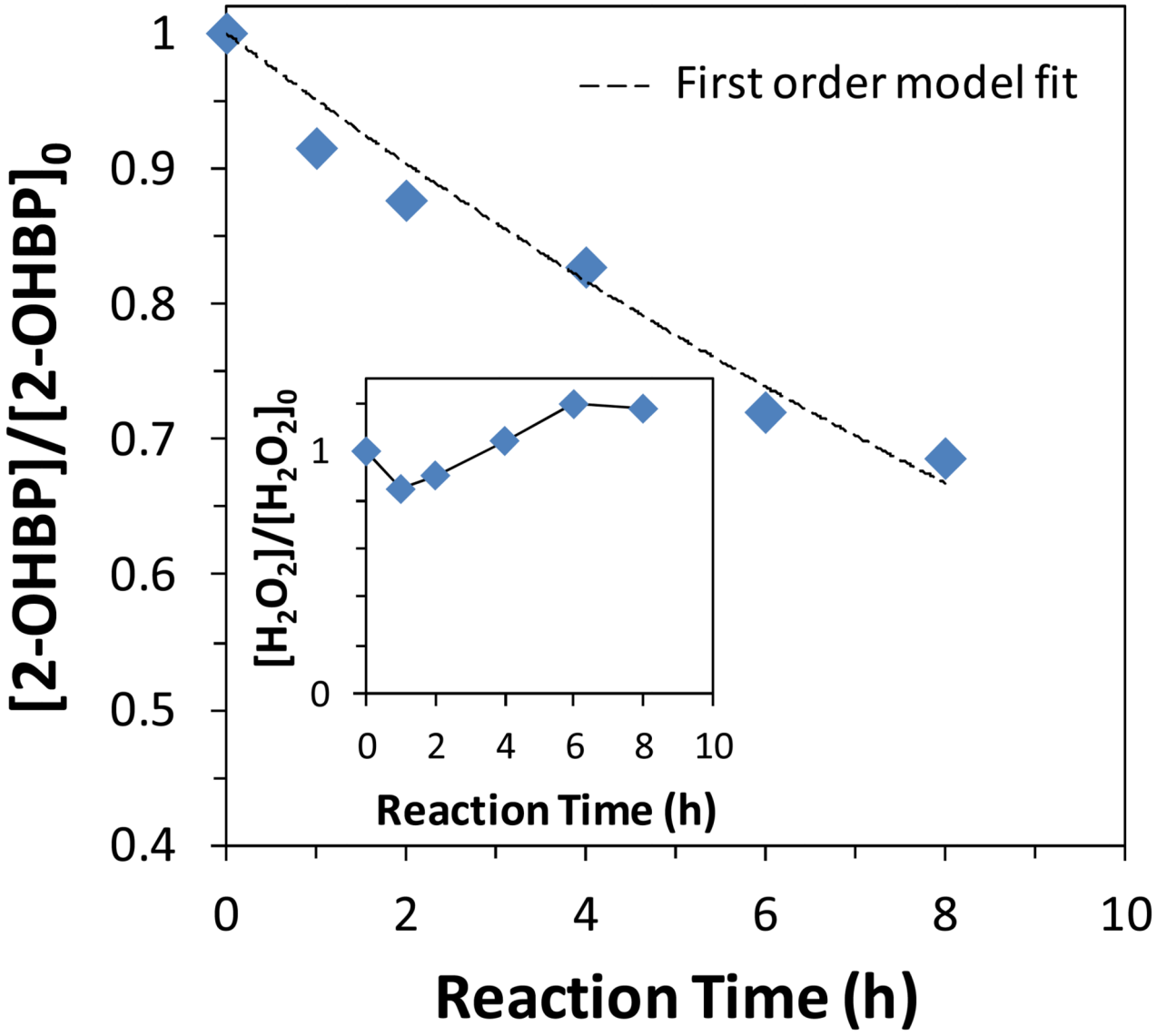

Figure 10.

2-Hydroxybiphenyl (2-OHBP) oxidation by iron oxide NPs. The inset was the H_2O_2 concentration (maintained constant) during the reaction. [Iron oxide]=0.5 g/L (BET surface area: 235 m^2/g), $[2\text{-hydroxybiphenyl}]_0$=0.43 mM, $[H_2O_2]_0$=50 mM. pH decreased from 6.9 to 5.1.

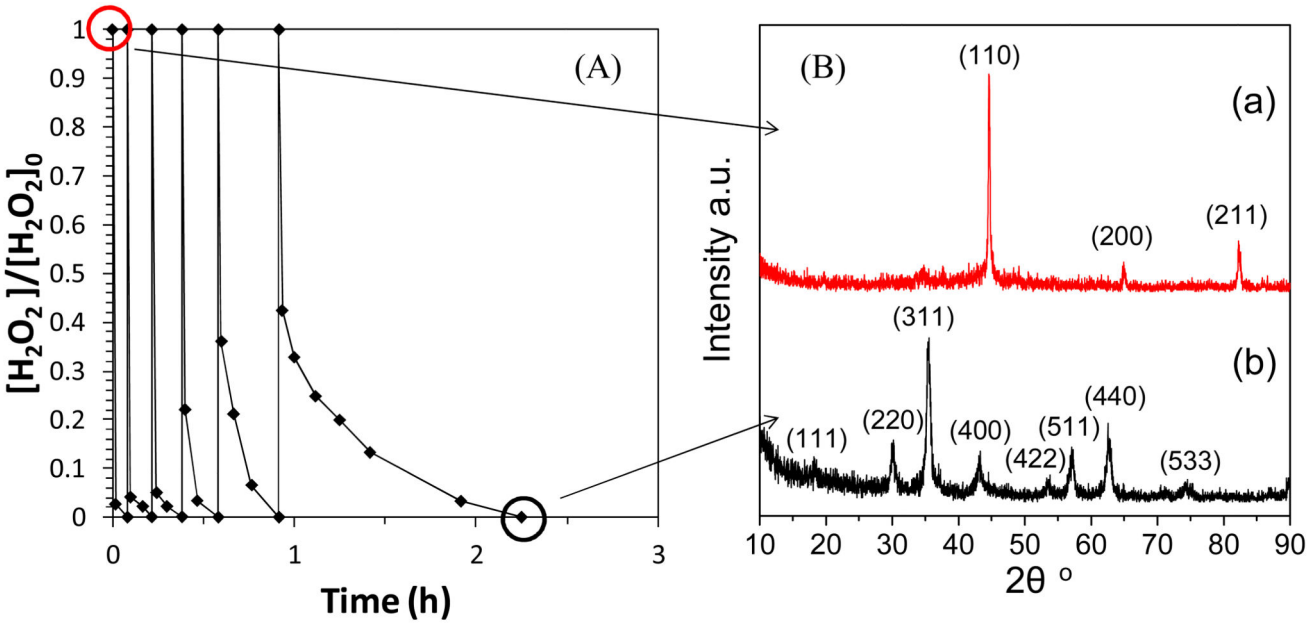

Figure 11.

H_2O_2 decomposition with Fe NPs (6 cycles). (A) H_2O_2 degradation; (B) iron transformation during the treatment. XRD spectra of Fe NPs before and after H_2O_2 treatment are shown in (a) and (b), respectively. [Fe]=20 mM, [H_2O_2] (each cycle)=4.4 mM, V=200 mL, pH=7.0–7.2. BET surface area (m^2/g): 37.8 (Fe) and 53.0 (Fe_3O_4).

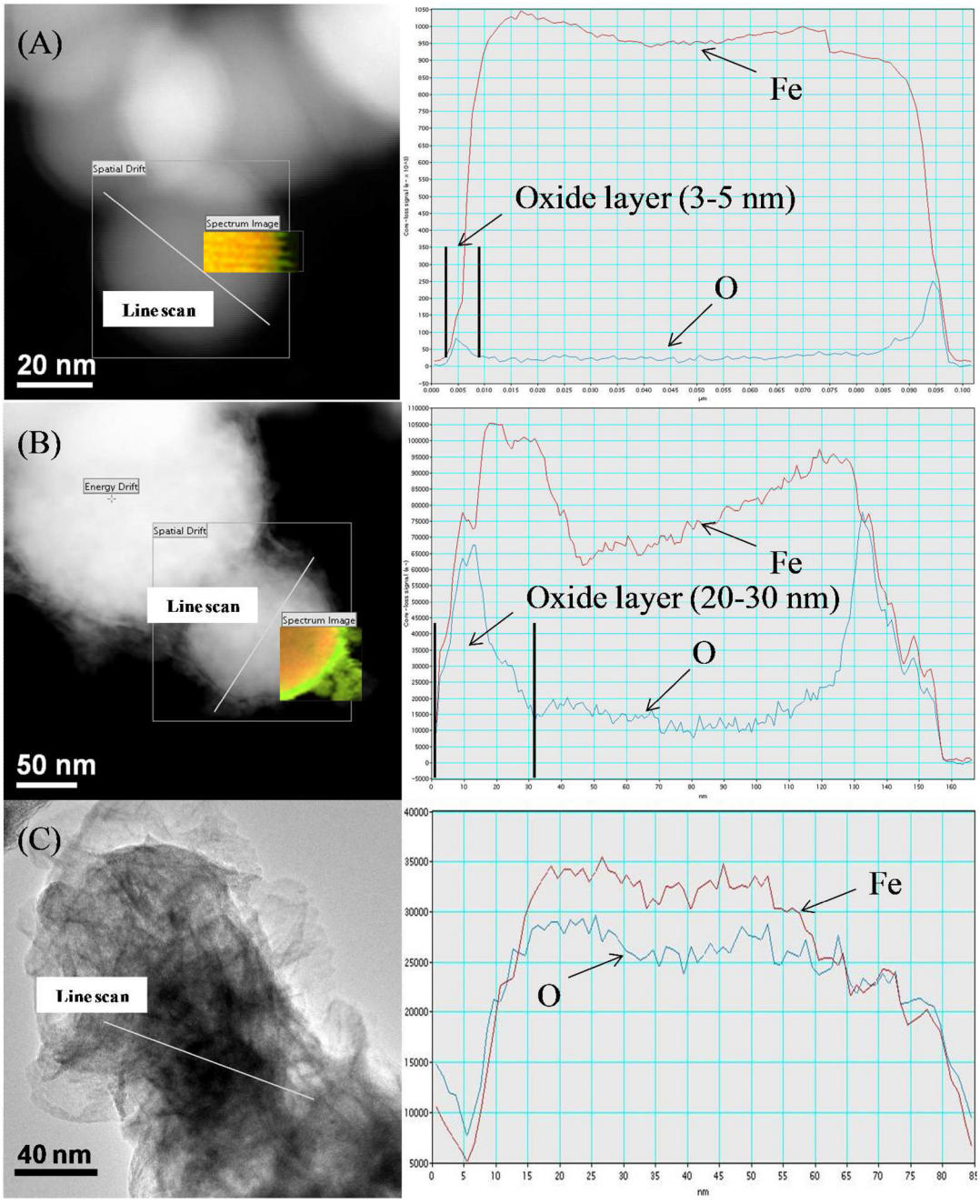

Figure 12.

STEM-EELS line scan and elemental mapping of Fe NPs during H_2O_2 oxidation. (A) Fresh Fe NPs; (B) Fe NPs after H_2O_2 treatment (1 cycle); (C) Fe NPs after H_2O_2 treatment (6 cycles). Yellow color indicates elemental Fe and green color indicates elemental O.